PCCP

Accepted Manuscript

ROYAL SOCIETY OF CHEMISTRY

www.rsc.org/pccp

Manuscript prepared for *PCCP*
March 26th, 2015

PAMAM G4 dendrimers as inhibitors of the iron storage properties of Human L-chain Ferritin

M.B. Camarada[2,†], V. Márquez-Miranda[1,3,†], I. Araya-Durán[1,3], A. Yévenes[4], F. González-Nilo[1,3,5*]

[1]*Universidad Andres Bello, Facultad de Biología, Center for Bioinformatics and Integrative Biology (CBIB), Republica 239, Santiago, Chile*

[2]*Universidad Bernardo O Higgins, Laboratorio de Bionanotecnología, General Gana 1780, Santiago, Chile*

[3]*Fundación Fraunhofer Chile Research, M. Sánchez Fontecilla 310 piso 14, Las Condes, Chile*

[4]*Pontificia Universidad Católica de Chile, Facultad de Química, Av. Vicuña Mackenna 4860, Macul, Santiago*

[5] *Centro Interdisciplinario de Neurociencia de Valparaíso, Facultad de Ciencias, Universidad de Valparaíso, Valparaíso 2366103, Chile*

Abstract

Cationic dendrimers, such as PAMAM, are known to be positively charged at neutral pH allowing their unspecific interaction with proteins and other cellular components. Specially, ferritin, that has an important role in iron homeostasis, presents a negative electrostatic potential at the 3-fold channel. This channel is important in the functionality of ferritin because it allows the iron entry into its inner cavity. In this way, it is expected the interaction between the protonated terminal amines of the dendrimer and the negative charged 3-fold channels of ferritin. Experimental measurements demonstrated that PAMAM G4 inhibits the iron storage properties of L-chain human ferritin (L-Ftn). Molecular dynamics simulations has been used to analyze the specific interaction between PAMAM G4 and L-Ftn. Results shown that PAMAM G4 effectively interacts with the 3-fold channels of L-Ftn, suggesting that this interaction is responsible of the inhibition of iron storage properties of L-Ftn.

Keywords: PAMAM G4, Apo L-Ferritin, molecular dynamics, channel blocker.

**e-mail: fernando.gonzalez@unab.cl*

†: *Both authors contributed equally to this work*

1. Introduction

Dendrimers are globular nanoscale macromolecules characterized by a strictly controlled structure, definite molecular weight, monodispersity, and biocompatibility[1]. In contrast to traditional linear polymers, they have a dendritically branched structure and consist of a core, separate branches and terminal functional groups[2] (Figure 1a). Polyamido-amine (PAMAM) dendrimers, which bear amide functionalities as repeating units, primary amines on the dendrimer terminals and tertiary amines in the interior, are an important class of dendrimers that have been used with increasing frequency as delivery systems of biologically active compounds into cells[3] and also for the controlled release of drugs[4, 5]. Dendrimers have the ability of forming conjugates and complexes with different substances due to either encapsulation into the inner cavities or interaction with the surface terminal amine groups. Hydrogen bonding, ionic, or hydrophobic interactions provide a platform for conjugation of the drug and targeting moieties like, oligonucleotides, nucleic acids, peptide, proteins and oligosaccharides[6-9].

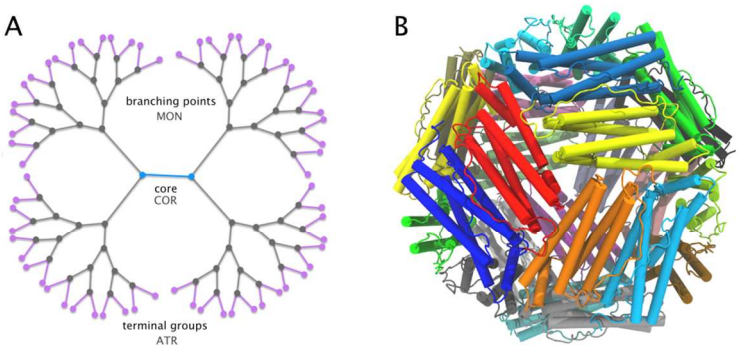

Figure 1: a) Amino terminated PAMAM G4 structure showing its main fragments and b) the structure of the protein L-Ftn showing one of its eight 3-fold channels.

Among available dendrimers, PAMAM G4 with a diameter of 45 Å[10], has been reported to have lower cytotoxicity in comparison to other larger generations of amino terminated PAMAM and has been successfully applied as a drug delivery system *in vitro* and *in vivo*[11]. However at physiological pH, primary external amines of PAMAM remain protonated[12, 13], allowing its unspecific interaction with proteins and other cellular components[14]. Furthermore, it has been shown previously that dendrimers might interact with bovine serum albumin (BSA); which are the most abundant proteins in plasma, and their interaction with these proteins is higher when the terminal groups are positively charged, unlike they are negative or neutral[15].

Specifically the protein Ferritin (Ftn), that has an important role in iron homeostasis[16, 17], presents a negative electrostatic potential, which could favor the development of unfavorable interactions with amino protonated groups of PAMAM G4.

Ferritins are ubiquitous iron-storage structures that are present in all kingdoms of life and are responsible of maintaining iron in a non-toxic but available form for cellular requirements[16]. Animal ferritins consist of two related subunits, heavy and light chain, H and L respectively, that assembles in different proportions to form the 24-subunit protein cage[18]. The H-chain contains a highly conserved catalytic center called the ferroxidase center (FC) that oxidizes Fe(II) to Fe(III) as the initial step of iron mineralization[16]. The Ferritin L-chain differs from H-chain in that it lacks of a FC and has metal-coordinating amino acid residues that are found on the internal surface of the assembled Ferritin, which play a significant role in the formation of stable iron mineral in animal Ferritins[19]. Iron incorporation into L-chain homopolymers of Ferritin in the absence of the FC has been shown *in vitro*. This occurs when iron binds and is oxidized at the nucleation site amino acids on the interior surface of Ferritins[20]. Despite of this difference between L and H chain of Ferritin, both share the same structure of the 3-fold channel; the iron entry route to its inner cavity[17]. Specifically, the human apo L-Ferritin (L-Ftn, Figure 1b) carries a negative net charge on their outer surface at neutral pH (isoelectric point pI 5.3)[21, 22]. Electronic density is not uniformly distributed, rather it is located in large negatively patches corresponding to eight negative spots around the pores along the three-fold symmetry axes[17].

As already pointed, at neutral pH PAMAM G4 has sixty-four amino protonated terminal groups. The presence of negative surface patches on L-Ftn, i.e. the eight 3-fold channels, can further guide and facilitate the formation of electrostatic interactions with the protonated amines and result in a stable PAMAM-Ferritin complex. Previous studies performed by Kostiainen and co-workers with viruses and protein cages such as ferritin, have experimentally demonstrated their good and stable interaction with amino terminated dendrons[23, 24]. Recent computational works have also described the self-assembly of nanostructures through electrostatic interactions[25, 26], suggesting that PAMAM dendrimers can effectively form stable complexes with Ferritin.

In order to study the interaction between PAMAM G4 and L-Ftn, experimental and theoretical explorations were proposed to analyze in detail the interaction between both systems and evaluate the performance of PAMAM G4 as possible blocker of 3-fold channels in Ferritin.

At the first section of this work, experimental assays were accomplished by UV-vis spectroscopy to study the effect of PAMAM G4 on the iron storage properties of L-Ftn and therefore, confirm the interaction between the dendrimer and the 3-fold channels present in L-Ftn. Our results showed that

PAMAM G4 effectively reduces the iron storage capacity of L-Ftn. In the second section of this manuscript, the blocking capacity of the dendrimer was evaluated through molecular dynamics tools. Computational simulations provided relevant information about structural interaction between the dendrimer and the protein, the residues involved in the non-covalent contacts and the stability of the complex. All results confirmed that PAMAM G4 effectively blocks the 3-fold channels of L-Ftn.

2. Materials and methods

2.1. Materials

Ferene, 2,2-bipyridyl, 3-(N-morpholino)propane sulfonic acid (MOPS), phenylmethane sulfonyl fluoride (PMSF), thioglycolic acid, uranyl acetate, ammonium acetate and ampicillin were purchased from Sigma Chemicals Company. Sodium chloride and ascorbic acid were procured from Merck, isopropyl-β-D-thiogalactoside (IPTG) and streptomycin sulfate from Invitrogen and tryptone and yeast extract from HIMEDIA. PAMAM G4 dendrimer (ethylenediamine core) was purchased from Sigma-Aldrich (St. Louis, MO).

2.2. Expression and purification

The gene of L-Ftn cloned in pDS20Trp-LFtn[27] was digested with *Nde*I and *BamH*1 and cloned in the expression vector pET3a (Novagen) to obtain the recombinant plasmid and transformed in *E. coli* strain BL21(DE3). The gene was sequenced to verify that no mutations were introduced. The *E. coli* BL21(DE3) containing the gene of L-Ftn was grown in LB medium(10 g of tryptone per liter, 10 g of NaCl per liter, 5 g of yeast extract per liter) with 100 mg/mL of ampicillin at 37 ºC to an optical density of 0.3-0.5 and then induced with 1mM of IPTG for 3 h at 37 ºC. The cells were harvested by centrifugation (~6 g from a 2 L culture), re-suspended in 7 mL of lysis buffer (100 mM MOPS pH 7.5; 0.2 mM PMSF), and sonicated four times for 15 s followed by 30 s on ice. The sonicate was centrifuged at 11,000g for 15 min at 4 ºC, then the supernatant fluid was heated to 75 ºC for 10 min followed by a second centrifugation step at 11,000g for 20 min at4 ºC. The protein solution was analyzed by SDS-PAGE.

2.3. Iron loading

In order to analyze the effect of PAMAM G4 on the ability of L-Ftn to store iron, the Apo form of the protein (0.2 μM) prepared as described by Treffry and Harrison[28], was incubated with and without 1.6 μM of PAMAM G4 in 100 mM MOPS pH 7. Then, the Fe(II) was added from a $FeSO_4$ stock solution prepared in 1 mM HCl to attain the desired iron concentration. Aliquots of 5 μM Fe(II)/cage were added every 10 min in successive steps until the sample reached a concentration of 50 μM Fe(II). Then, the samples were incubated at room temperature by 6 hours and left at 4 °C overnight. The samples were then centrifuged and dialyzed with 100 mM MOPS pH 7 for 24 h. The iron storage in L-Ftn was analyzed by the Ferene method[29].

2.4. Molecular Simulation details

In order to study the structural interaction between PAMAM G4 and L-Ferritin, molecular dynamics (MD) simulations were run using an isobaric-isothermal (NPT) ensemble, where the number of particles, the pressure and the temperature were held constant. A Langevin thermostat was employed to keep a mean temperature of 298 K and Langevin piston[30] method was considered to maintain a mean pressure of 1 atm. All molecular dynamics simulations were performed using the computational code NAMD[31]. Systems underwent 2000 steps of energy minimization followed by 100 ns of dynamics in the case of the L-Ftn/PAMAM G4 system, 2 ns for the isolated dendrimer and 4 ns for the protein system. Apo L-Ftn structure (PDB ID: 2FG8)[32] was obtained from Protein Data Bank website (http://www.rcsb.org/), and all alpha-carbon atoms were restrained along the simulations (1 kcal/mol·Å).

The equations of motion were integrated with a 2.0 fs time step along with SETTLE[33] and RATTLE[34] to constrain the geometry of the water molecules and the length of covalent bonds to hydrogen atoms. Non-bonded energies were calculated using particle-mesh Ewald full electrostatics[35] (grid spacing < 0.10 nm). Long-range electrostatic interactions were calculated every 2 steps using a multiple-time stepping scheme. Interactions among aminoacids, ions, and TIP3P water molecules[36] were computed using the CHARMM27 force field[37, 38].

All simulation systems were cubic in shape, and periodic boundary conditions were enforced in all three directions. A suitable amount of ions was added to each simulation box to ensure neutrality of the system: Na^+ and Cl^- ions in the case of L-Ftn/PAMAM G4 system and the isolated protein, and Cl^- ions for the isolated dendrimer.

In order to generate parameters to describe interactions involving the atoms of PAMAM G4, it was necessary to parameterize its structure because it is not included in conventional force fields. To

parameterize the dendrimer, its structure was divided into three segments as Figure 1a shows: the ethylenediamine core named COR, intermediate dendrons named MON and the outer surface with protonated terminal amines, named ATR. The molecular geometry of each segment was optimized using the Gaussian 03 software package[39]. Each segment was parametrized separately, and the segments were later assembled to form a complete dendrimer. Thus, considering the organic nature of PAMAM dendrimer, parameters and topology for each segment were obtained from CHARMM General Force Field (CGenFF)[40] and PARAMCHEM website (http://www.paramchem.org)[41, 42] in accordance with CHARMM27 philosophy. As already mentioned, at physiological pH the terminal primary amines remain protonated, while the intermediate dendrons and core has neutral amines. Conventional classical MD is incapable of reproducing protonation and deprotonation of certain groups along the simulation; it is impossible to fix a pH ensemble. Therefore, to reproduce experimental conditions, each one of the 64 terminal amines in the molecular model of the dendrimer was set to a positive charge of +1e.

3. Results and discussion

3.1. Effect of PAMAM G4 on the iron storage properties of L-Ferritin

In order to analyze the effect of PAMAM G4 on the iron storage properties of ferritin, the Apo form of L-Ftn was incubated with Fe(II) in presence of this dendrimer. In general, aliquots of 5 μM Fe(II) were added to Apo L-Ftn solution (0.2 μM) in presence of 1.6 μM of PAMAM G4. L-Ftn has eight 3-fold channels where Fe(II) could enter to the protein, therefore a concentration of PAMAM G4 eight times larger than L-Ftn was used to perform the experiment. After iron incubation, the samples were characterized by UV-vis spectroscopy. Figure 2 shows that L-Ftn is able to store iron and keep it in solution. The presence of an inner iron core in L-Ftn produces an increase in the absorbance around 305 to 315 nm due to the charge transfer bands of O_2^-/OH^- coordinated Fe(III)[46] (Fig. 2). However, this is not the case by the control samples (iron alone and iron incubated with PAMAM G4) where the absence of absorbance around 305 to 315 nm indicates that iron is oxidized by dioxygen and precipitate as Fe(O)OH. Besides, the presence of PAMAM G4 produced a reduction in the intensity of the absorbance around 305 to 315 nm in comparison to the profile exhibited by L-Ftn incubated alone with iron, Fig. 2.

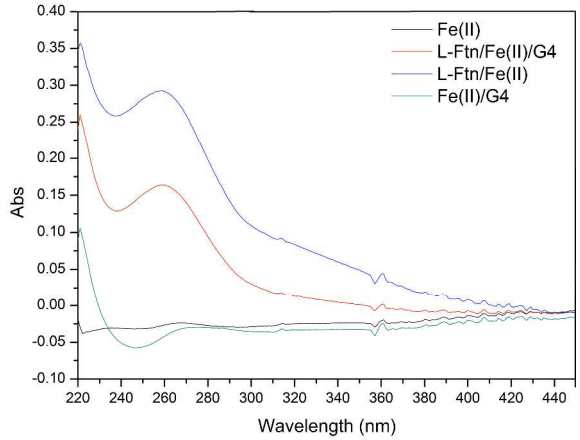

Figure 2: Absorbance spectrum of iron in the presence of PAMAM G4, L-Ftn and L-Ftn/PAMAM G4. Apo L-Ftn (0.2 μM) was incubated with and without 1.6 μM of PAMAM G4 in 100 mM MOPS pH 7. Aliquots of 5 μM Fe(II)/cage were added every 10 min in successive steps until the sample reached a concentration of 50 μM Fe(II) as described in Material and Methods.

In order to quantify the effect of PAMAM G4 on the iron storage properties of L-Ftn, the concentration of iron of each sample was measured by Ferene methods[29]. Detailed concentration values of Fe(II) at each sample are available in Table 1.

Table 1: Concentration of Fe(II) in each sample quantified by the Ferene method. The Fe(II) concentration is shown as mean ± SD. The data represent the average of four separate reactions.

	Fe(II) (μM)
Fe(II) 50 μM	0.4 ± 0.2
L-Ftn 0.2 μM / Fe (II) 50 μM / PAMAM G4 1.6 μM	6.3 ± 0.9
L-Ftn 0.2 μM /Fe(II) 50 μM	29 ± 6.0
Fe(II) 50 μM / PAMAM G4 1.6 μM	3.6 ± 1.2

Figure 3 shows that approximately 60% of the added amount of iron was stored inside the protein. However, a decrease in the total iron storage by L-Ftn was observed in the presence of PAMAM G4. Considering that PAMAM G4 coordinated approximately 3.6 μM of Fe(II), the total iron storage in L-Ftn decreased about 90 % in comparison to the L-Ftn/Fe(II) system.

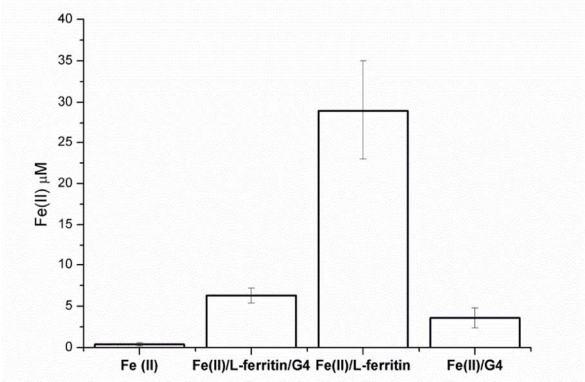

Figure 3: Quantification of the total amount of iron storage by L-Ftn in presence of PAMAM G4. The iron presence in each sample show in Fig. 2 was determined by the Ferene method[30].

This result suggests that PAMAM G4 blocked the 3-fold channels present in the structure of L-Ftn, hindering the entrance of Fe(II). Besides, PAMAM G4 can bind a low concentration of Fe(II). In relation to this, it has been reported that PAMAM type dendrimers form stable complexes with Fe(II)[43-45]. However, metal ion binding to PAMAM dendrimers is pH dependent; at low pH values (pH<3.5), all amine sites of PAMAM are protonated[46] and protons effectively compete with metal cations for the coordination sites[47]. Progressive penetration of metal ions into the dendrimer only occurs with an increase in pH. At pH values higher than 5, terminal amine groups remain charged, but internal amines deprotonate giving rise to the formation of complexes at the core site[48]. In this study, terminal charged amine groups disfavor initial coordination and progressive penetration of Fe(II) ion into the core site; protonated amines hinder the traveling of Fe(II) ions toward internal sites of the dendrimer such as the amide site, or eventually the core of the ligand.

3.2. Computational simulation

Considering the experimental results, molecular dynamics simulations were run with the aim of characterizing the structural interaction between PAMAM G4 and L-Ftn. In order to evaluate the blocking mechanism of PAMAM G4 one molecule of dendrimer was located at 15 Å from one of the eight 3-fold channels present at the protein. A preliminary phase of MD in NPT conditions for PAMAM G4 and L-Ftn structures was used to pre-equilibrate and relax the dendrimer and ferritin in solution (2 ns and 4 ns respectively). The structural coordinates obtained after relaxation of PAMAM G4 and L-Ftn were used to build initial geometries of the system PAMAM G4/L-Ftn. All these simulations were run under Periodic Boundary Conditions (PBC) and using explicit water molecules (TIP3P[36]) as solvent.

3.2.1. Molecular simulations of PAMAM G4 and L-Ftn

As Figure 1Sa shows, after equilibration the PAMAM G4 system reached a stable energetic profile. The variation of the radius of gyration (R_{gyr}) along the simulations is also presented as Supporting Information (Figure 1Sb). The evolution of this quantity remained stable over the time, reaching a more compacted structure in comparison to the starting geometry. The mean value of R_{gyr} during the last 0.5 ns of simulation is 21.8 Å. This value is in agreement with experimental measurements performed by small angle neutron scattering (SANS)[49] for PAMAM G4 at neutral pH conditions (21.58 ± 0.41Å) and theoretical studies performed by Goddard III and coworkers[50] (21.43 Å).

As above-mentioned, the crystal structure of human L-Ftn chosen for this study was obtained from the protein data bank (PDB ID: 2FG8). After the neutralization of the system with ions, classical molecular dynamics simulation was run over 4 ns. Alpha-carbon atoms were restrained along the simulation. As Figure 2Sa shows, the protein reached a stable energetic profile after 0.2 ns and remain steady during the whole simulation. Also, after this time the evolution of R_{gyr} over the full trajectory remained remarkable steady over the time, indicating that the system converged with good stability.

3.2.2. Molecular simulation of L-Ftn /PAMAM G4

The structural coordinates of the last step of PAMAM G4 and L-Ftn simulations provided the initial geometries to start the PAMAM G4/L-Ftn simulation. In order to rapidly see interaction within the simulation, the dendrimer structure was manually positioned near to one of the 3-fold channels of L-Ftn while still having no atoms of the dendrimer closer than 10 Å from those of the protein (Figure 4a). The system was solvated and neutralized before running 100 ns of classical molecular dynamics simulation.

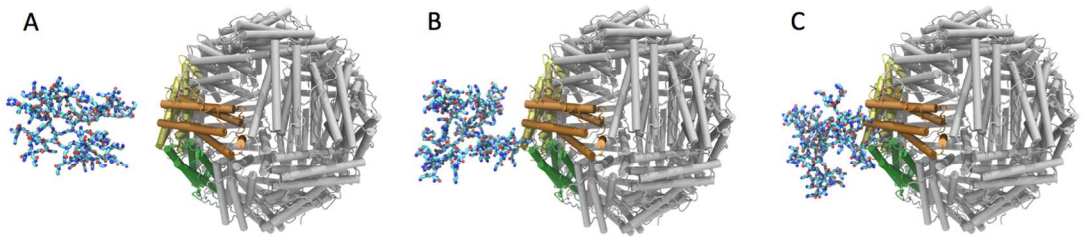

Figure 4: Snapshot of PAMAM G4/L-Ftn molecular simulation at a) the beginning of the simulation t=0, b) at t=4.5 ns and c) at the last step of simulation, t=100 ns. Chains that form the 3-fold channel (B, I and K) are highlighted in colors.

In order to characterize the energetic behavior of the system and to study its stability, different properties were followed along the simulation. The top row of Figure 5 shows the energetic interaction between the dendrimer and the L-Ftn during 100 ns. As expected, the most important contribution to the total energy is given by the electrostatic energy, which is directly related to the interactions between charged terminal amines of the dendrimer and negatively charged side chains of certain aminoacids. Consequently, this energetic profile has a leading role in the stabilization of the system. The total energy interaction remained quite stable till 4.5 ns of simulation time, where the plot shows an important decrease, i.e. the system became more stable.

At this point, the system was structurally characterized. As Figure 4b depicts, the terminal branch of the dendrimer, named ATR89, penetrated the 3-fold cavity formed by chains B, I and K, leading to the appearance of new interactions between both macromolecules that stabilized the system. At the same time, a second terminal branch, ATR88, settled at the entrance of the cavity interacting with the amino acids that conform the external part of the channel. Both branches remained next to the channel until the end of the simulation, as Figure 4c shows.

Once the dendrimer branch ATR89 was identified as the main blocker of the 3-fold channel, the distance of its terminal nitrogen atom to the center of mass (COM) of the 3-fold pore was plotted. This distance characterized the penetration of the branch of the dendrimer into the pore as simulation progressed. As Figure 5b shows, the dendrimer quickly moved closer to the 3-fold channel, to reach an average distance at 2.8 ns of 3.4 Å from the terminal nitrogen atom of the ATR89 branch to the COM of the 3-fold channel. This distance stayed rather stable until 45 ns. At t=46 ns, a new decrease in the distance to the COM center was registered, reaching an average distance of 2.5 Å. This reduction is related to a deeper penetration of the ATR89 branch into the 3-fold channel, which led to a newer total energetic decrease at around 60 ns. The later profile reached a steady behavior until the end of the simulation.

Figure 5c represents the evolution of the total number of hydrogen-bond (Hbond) contacts between the dendrimer and L-Ftn along the trajectory with a cutoff of 3 Å. As shown by the distance profile, at t=2.8 ns the total amount of these interactions intensely increased, demonstrating that the entrance of the branch to the 3-fold channel produced new and steady interactions between both molecules that induced the energetic stabilization of the system observed in Figure 5a.

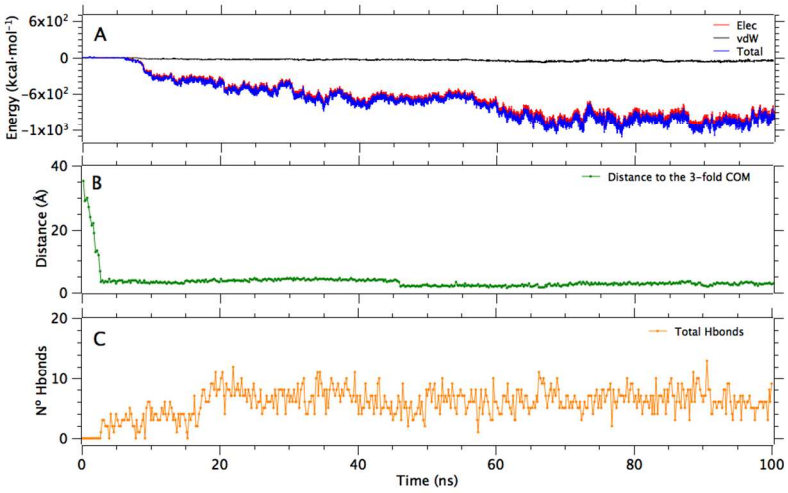

Figure 5: a) Energetic interaction between PAMAM G4 and L-Ftn during the simulation, b) distance from nitrogen atom of branch ATR89 to the COM of the 3-fold channel and c) total number of hydrogen-bond interactions between the dendrimer and the protein.

The stability of the number of hydrogen-bond interactions, along with the energetic interaction profile and the distance of the terminal nitrogen atom of the interacting branch ATR89 to the COM of the 3-fold channel, indicate that the interaction between PAMAM G4 and L-Ftn is quite stable over time, energetically predominated by electrostatic interactions. Once the dendrimer branch progressively approached to the protein and entered into the pore, the number of Hbond contacts between both molecules raised and remained stable during the simulation, accounting for the effective and constant interaction of the dendrimer with the L-Ftn 3-fold channel until the end of the simulation.

In order to provide deep insights about the Hbond interactions, contacts between the dendrimer and L-Ftn were obtained in detailed along of the MD simulation. Table 2 summarizes the interactions between the dendrimer terminal branches (ATR) and some specific residues of the protein. Only Hbond interactions between terminal branches of PAMAM G4 and the protein were detected. The percentage of occupancy (% occupancy) represents the proportion of time while the interactions persisted during the total time of simulation. Only those Hbond interactions with a percentage of occupancy higher than 20% were considered in this analysis.

As Table 2 indicates, Hbond interactions between both macromolecules were detected only with those protein chains that conform the 3-fold channel (B, I and K). The interactions between the external surface of the pore and non-blocking dendrimer branches (ATR84 and ATR87) presented the highest prevalence during the simulation, with a percentage of occupancy near 85%.

Table 2: Summary of HBond interactions between terminal branches ATR (see Figure 1a for fragments labeling) of PAMAM G4 and L-Ftn along the MD simulation.

Branch	Protein chain	Residue	% occupancy
ATR89	B	Asp 131	49.8
ATR89	I	Glu 134	22.9
ATR89	K	Glu 134	23.7
ATR88	B	His 118	23.1
ATR84	K	Asp 15	82.7
ATR87	I	Asp 116	87.5
ATR116	B	Asp 15	26.3
ATR85	K	Asp 116	30.5
ATR79	I	Asp 15	21.3
ATR93	B	Asp 116	34.5

Therefore, both non-blocking and blocking dendrimer branches have a significant role in the stabilization of the interaction between PAMAM G4 and L-Ftn during the whole molecular dynamic simulation. The residues involved in Hbonds interactions are Asp, Glu and His. Asp and Glu are the only amino acids with acidic characteristics. Their side chains have carboxylic acid groups whose pKa's are low enough to lose protons, becoming negatively charged in the process. Thus, the terminal protonated amines of PAMAM G4 preferably interact with these residues. His is the only basic amino acid that interacts with the dendrimer. Even though histidine at neutral pH has a charged amine group, it has a second amine at the aromatic cycle, capable of interacting with the terminal amine groups of PAMAM G4.

The evolution of each Hbond interaction was followed along the entire simulation. Figure 6a shows Hbond interactions between ATR88 and ATR89 branches that penetrated into the 3-fold channel, while Figure 6b follows the development of these kind of interactions between the entire dendrimer structure and L-Ftn.

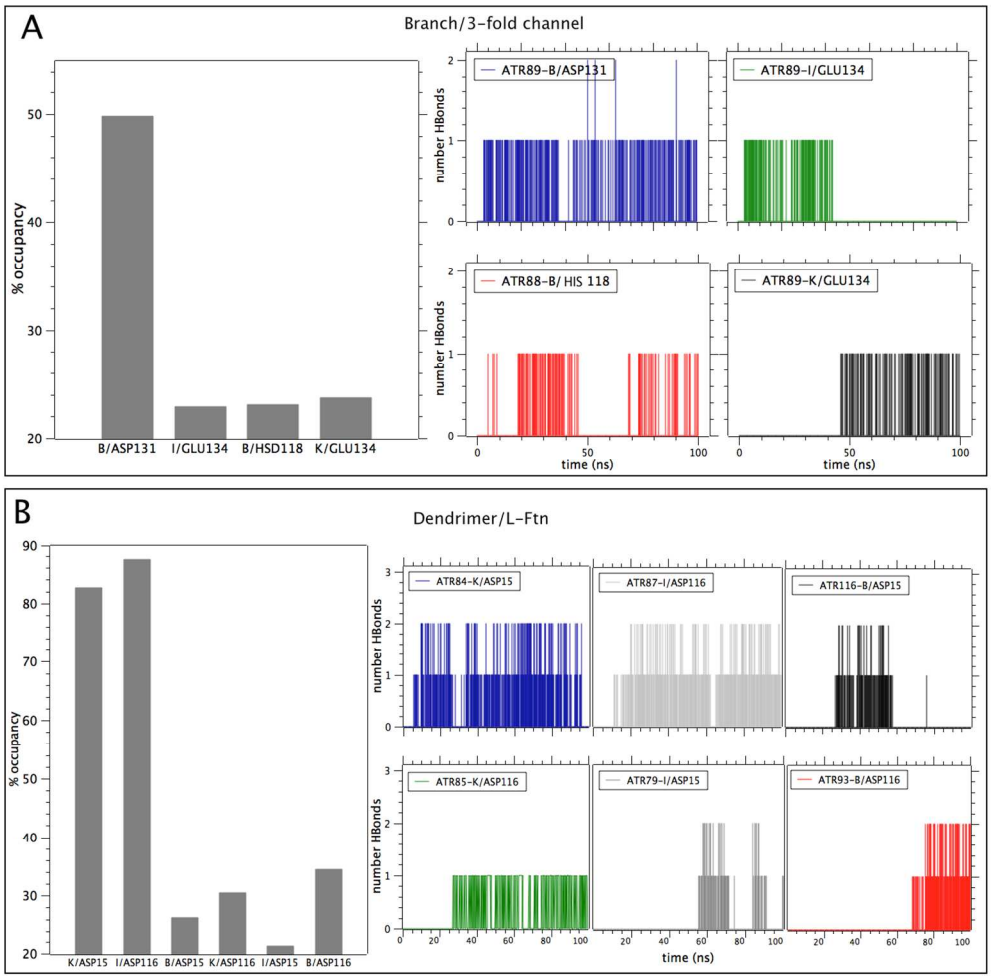

Figure 6: Percentage of occupancy and evolution of Hbond type interactions between a) the interacting branches (ATR88 and ATR89) and the 3-fold channel of L-Ftn and b) between the whole structure of PAMAM G4 and L-Ftn.

As can be seen at Figure 6a, the interaction ATR89/B-Asp 131 is the most prevalent with almost 50% of occupancy. The later contact together with ATR89/I-Glu 134 is the first to appear at approximately 2.8 ns, the same time at the dendrimer reduced its distance to the COM of the 3-fold channel. As already mentioned, branch ATR88 settled at the entrance of the 3-fold channel during the simulation and interacted with the neutral amine group present at His 118 aromatic ring with an occupancy percentage of 23.1%. This amino acid is located at the beginning of the pore and together with residue B-Asp 131 facilitated the initial attachment of the dendrimer to the 3-fold channel. At t=45 ns, the ATR89/I-Glu 134 interaction disappeared, but at the same time, a new contact was generated with residue K-Glu134 coinciding with the deeper and definitive penetration of the branch ATR89 into the 3-fold channel as pointed in Figure 5b. Figure 7 depicts snapshots of

each of the Hbond interactions between the dendrimer branches ATR88 and ATR89 and the 3-fold channel.

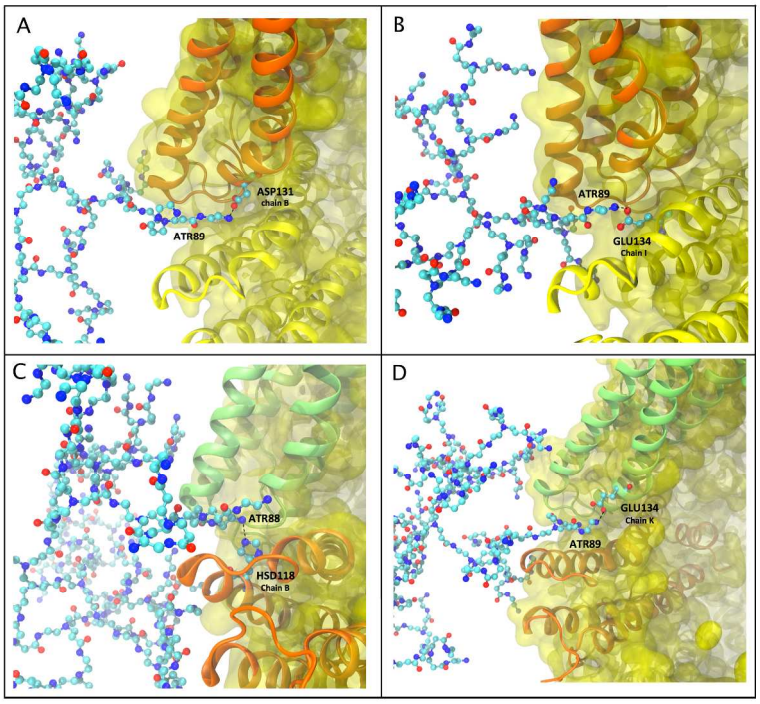

Figure 7: Snapshots of the HBond type interactions between terminal branches ATR88 and ATR89 and the 3-fold channel.

On the other hand, as Figure 6b displays, the interaction between the dendrimer and L-Ftn was registered only with aspartic acid residues located at the external side of the 3-fold channel as Figure 8 shows. As already pointed, the most prevalent interactions correspond to I-Asp 116 and K-Asp 15. From t=30 ns, one new interaction between ATR85 and K-Asp 116 was registered, remaining stable until the end of the simulation. In addition, from 60 ns there was an increase in the total number of interactions with the terminal branches of the dendrimer and residues B-Asp 15, I-Asp 15 and B-Asp 116. This fact is directly related to the stabilization of the total energy interaction shown in Figure 5a that started at this simulation time.

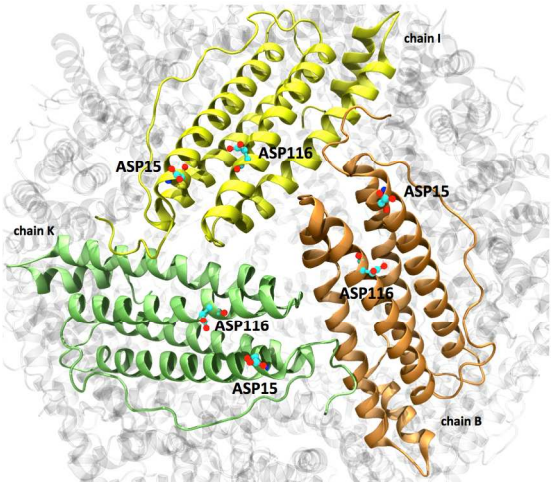

Figure 8: Aspartic acid residues located at the surface of L-Ftn, involved in the Hbond interactions with PAMAM G4 dendrimer.

With the aim of measuring the stability degree of the interaction between the dendrimer and L-Ftn from a structural point of view, different characterization analyses were performed to compare the system before and after to the penetration of PAMAM G4 branch into L-Ftn. To describe how Ferritin is altered due to the entrance of PAMAM dendrimer branch, the radial distribution function (RDF) of L-Ftn, PAMAM G4 dendrimer, Na^+ ions and water was plotted with respect to the distance to the protein center-of-mass (COM). Two different stages of simulation were considered: t=0.5 ns, were the dendrimer is still at an unbound state, and the last fragment of the MD trajectory with a L-Ftn/PAMAM G4 complex.

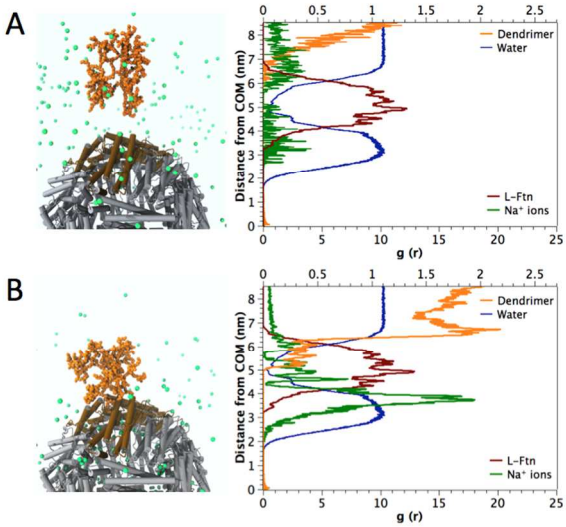

Figure 9. RDF profiles of L-Ftn 3-fold channel, PAMAM-G4 dendrimer, Na^+ ions and water, obtained from the first part of the trajectory (A, unbound state) and from the last fragment (B, bound state) when the dendrimer is blocking the pore.

As Figure 9 shows, the dendrimer appears as a dense core when it is close to the protein, i.e. at the bound state. Since L-Ftn is a hollow shell, water density in the center of the protein is similar to the bulk density. On the other hand, the positive sodium ions are capable of interacting with the negative density of the 3-fold channels belonging to L-Ftn. Therefore, Na^+ distribution can deliver relevant information on how the entrance of the dendrimer branch displace these ions in order to favor the interaction with the protonated terminal groups of PAMAM G4. The distribution of sodium ions (distance from COM ~ 6-8 nm) in the vicinity of the 3-fold channel (represented by the peak of L-Ftn, distance 3.5 - 6.5 nm) is lower in the bound state in comparison to the starting stage of the simulation, due to the effect of the dendrimer branch binding the pore. The high peak of Na^+ (density at distance from COM ~ 2-4 nm) is clear evidence that the flux of ions through the 3-fold channel has diminished because of the branch entrance, so they are accumulated in the center of the protein once they have penetrated through another pores.

The new electrostatic interaction between the protonated amino groups of the dendrimer branch and the 3-fold channel is related with the number of salt bridges. As Figure 3S depicts, once PAMAM G4 branch is attached to the pore, the number of electrostatic interactions remains stable until the end of the simulation, as well as the number of hydrogen bonds. During the last 5ns of simulation, the electrostatic interaction between both segments represents the 53% of the total interaction (Hbonds + salt bridges), showing that this kind of forces are very important in the stabilization of the system.

The radius of gyration (R_{gyr}) and the root-mean-square deviation (RMSD) of the dendrimer branch ATR89 that penetrates into the 3-fold channel was also measured and compared with a non-interacting dendrimer branch. As Figure 10 shows, the RMSD and R_{gyr} plots belonging to the non-interacting dendrimer branch show oscillating profiles with higher deviation in comparison to the interacting branch ATR89. The profiles that belong to the penetrating branch get rapidly stabilized and reach a constant behavior as the simulation time progressed.

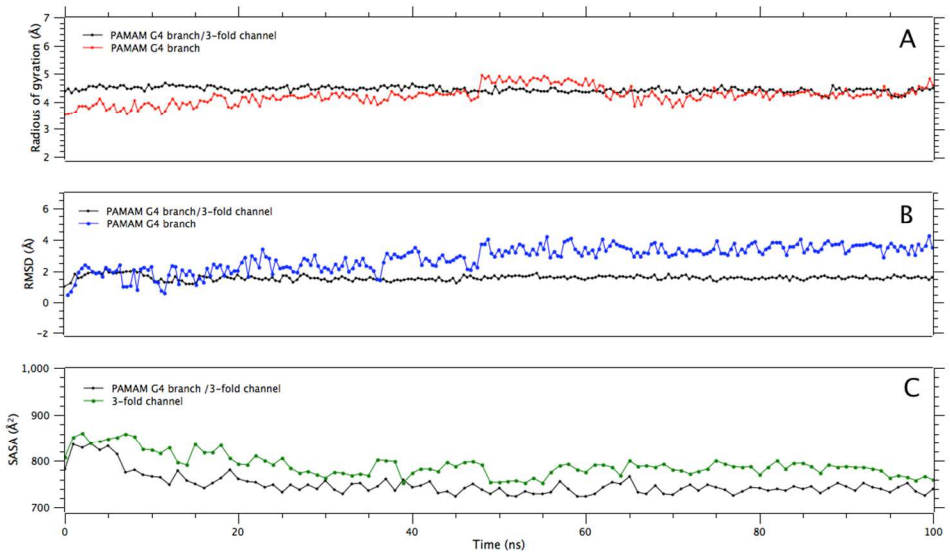

Figure 10: a) Radius of gyration, b) root-mean-square deviation (RMSD) of a branch of PAMAM G4 interacting and not interacting with the 3-fold channel of L-Ftn and c) surface accessible solvent area (SASA) of a free 3-fold channel and a 3-fold channel being blocked by PAMAM G4.

The surface accessible solvent area (SASA) was also plotted for an interacting and non-interacting 3-fold channel of L-Ftn with dendrimer branches (Figure 10c). Before t=2.8 ns, while the dendrimer is still enough separated from the protein, SASA exhibit very similar values for both pores. However, in the case of the interacting pore, this value progressively decays until t=46 ns, when reaches a mean value of 703 $Å^2$. As shown at Figure 5b, at this time there was a decrease in the distance of the terminal amine of ATR89 to the COM of the pore, reaching the lowest average value of distance during the molecular dynamic simulation and therefore producing a diminution in the SASA values.

The profiles displayed in Figure 10 demonstrate that electrostatic interactions together with hydrogen-bond contacts effectively hold up the dendrimer to the 3-fold channel of L-Ftn. The stability of PAMAM/protein complex during the time of simulation confirms that PAMAM G4 is an effective blocker of 3-fold channels in L-Ftn.

This study characterized at atomic level dendrimer-Ftn complexes. All results demonstrated that PAMAM G4 effectively interacts and blocks the 3-fold channels of L-Ftn, reducing the iron storage capacity of this protein. Therefore, PAMAM G4 dendrimers could affect negatively iron homeostasis.

4. Conclusions

In this work, the chemical interactions between PAMAM G4 and L-Ftn were studied. Experimental measurements demonstrated that PAMAM G4 effectively inhibits the iron storage properties of L-Ftn. The molecular dynamics analysis shows that PAMAM G4 interact with the 3-fold channel of L-Ftn, suggesting that this interaction is responsible by the low iron storage properties of L-Ftn in presence of PAMAM G4. Computational approaches confirmed the relevance of electrostatic interactions on the stabilization of the system PAMAM G4/L-Ftn. H-Bond type interactions preferentially between the terminal protonated amino groups of the dendrimer and acidic amino acids such as Glu and Asp contributed greatly to the permanent blockage of the channel from the first contact between both molecules, till the end of the simulation. Both superficial and inner-channel interactions were stable along the simulation, confirming that PAMAM G4 acts as an effective channel blocker of L-Ftn. This study, suggest that amino terminated dendrimers can affect the iron metabolism. To efficiently address this issue, it could be an option to develop a new dendrimer which keeps the ability to bind nucleic acids and also, avoid its non-specific interaction with plasma proteins, by modulating the charge of its terminal groups and introducing neutral molecules.

Acknowledgements

M.B.C. is grateful to Fondecyt for financial support (Initiation Project nº 11140107). V.M.M. thanks Conicyt for a PhD Scholarship and CONICYT + PAI/ "Concurso Nacional Tesis de Doctorado en la Empresa" 2014 (781413007). D.G.N., V.M. and I.A. thank for support of Fraunhofer Chile Research, Innova-Chile CORFO (FCR-CSB 09CEII-6991) and Anillo Científico ACT1107. The Centro Interdisciplinario de Neurociencia de Valparaíso (CINV) is a Millennium Institute supported by the Millennium Scientific Initiative of the Ministerio de Economía, Fomento y Turismo.

References

1. Tomalia, D. A.; Baker, H.; Dewald, J.; Hall, M.; Kallos, G.; Martin, S.; Roeck, J.; Ryder, J.; Smith, P. *Polym. J.* **1985,** 17, 117-132.
2. Fréchet, J. M. J.; Tomalia, D. A., *Dendrimers and Other Dendritic Polymers.* John Wiley & Sons: Chichester, New York, USA, 2001.
3. Aulenta, F.; Hayes, W.; Rannard, S. *European Polymer Journal* **2003,** 39, (9), 1741-1771.
4. Esfand, R.; Tomalia, D. A. *Drug Discovery Today* **2001,** 6, 427–436.
5. Svenson, S.; Tomalia, D. A. *Adv. Drug. Deliv. Rev.* **2005,** 57, 2106-2129.

6. Boas, U.; Heegaard, P. M. H. *Chem. Soc. Rev.* **2004,** 33, 43-63.
7. Bhadra, D.; Yadav, A. K.; Bhadra, S.; Jain, N. K. *Int. J. Pharm.* **2005,** 295, 221-233.
8. Kono, K.; Liu, M.; Fréchet, J. M. *Bioconjugate Chemistry* **1999,** 10, 1115-1121.
9. Kesharwani, P.; Keerti, J.; Kumar, N. *Progress in Polymer Science* **2014,** 39, 268–307.
10. Domański, D. M.; Klajnert, B.; Bryszewska, M. *Bioelectrochemistry* **2004,** 63, (1–2), 189-191.
11. Choksi, A.; Sarojini, K. V. L.; Vadnal, P.; Dias, C.; Suresh, P. K.; Khandare, J. *International Journal of Pharmaceutics* **2013,** 449, (1–2), 28-36.
12. Cakara, D.; Kleimann, J.; Borkovec, M. *Macromolecules* **2003,** 36, (11), 4201-4207.
13. Karatasos, K.; Posocco, P.; Laurini, E.; Pricl, S. *Macromolecular Bioscience* **2012,** 12, (2), 225-240.
14. Shen, Y.; Zhou, Z.; Sui, M.; Tang, J.; Xu, P.; Kirk, E. A. V.; Murdoch, W. J.; Fan, M.; Radosz, M. *Nanomedicine* **2010,** 5, (8), 1205-1217.
15. Klajnert, B.; Stanisławska, L.; Bryszewska, M.; Pałecz, B. *Biochimica et Biophysica Acta (BBA) - Proteins and Proteomics* **2003,** 1648, (1–2), 115-126.
16. Le Brun, N. E.; Crow, A.; Murphy, M. E.; Mauk, A. G.; Moore, G. R. *Biochim. Biophys. Acta* **2010,** 1800, 732-744.
17. Behera, R. K.; Theil, E. C. *Proc. Natl. Acad. Sci. USA* **2014,** 111, 7925-7930.
18. Granier, T.; Gallois, B.; Dautant, A.; Langlois d'Estaintot, B.; Precigoux, G. *Acta Crystallogr. D Biol. Crystallogr.* **1997,** 53, 580-587.
19. Santambrogio, P.; Levi, S.; Cozzi, A.; Corsi, B.; Arosio, P. *Biochem. J.* **1996,** 314, 139-144.
20. Levi, S.; Santambrogio, P.; Cozzi, A.; Rovida, E.; Corsi, B.; Tamborini, E.; Spada, S.; Albertini, A.; Arosio, P. *J. Mol. Biol.* **1994,** 238, 649-654.
21. Worwood, M., *Indicators of the iron status of populations: Ferritin*. 2nd ed.; World Health Organization, CDC.
: Geneva, 2007.
22. Bomford, A.; Berger, M.; Lis, Y.; Williams, R. *Biochemical and Biophysical Research Communications* **1978,** 83, (1), 334-341.
23. Kostiainen, M. A.; Ceci, P.; Fornara, M.; Hiekkataipale, P.; Kasyutich, O.; Nolte, R. J. M.; Cornelissen, J. J. L. M.; Desautels, R. D.; van Lierop, J. *ACS Nano* **2011,** 5, (8), 6394-6402.
24. Kostiainen, M. A.; Hiekkataipale, P.; de la Torre, J. A.; Nolte, R. J. M.; Cornelissen, J. J. L. M. *Journal of Materials Chemistry* **2011,** 21, (7), 2112-2117.
25. Garzoni, M.; Okuro, K.; Ishii, N.; Aida, T.; Pavan, G. M. *ACS Nano* **2014,** 8, (1), 904-914.
26. Doni, G.; Kostiainen, M. A.; Danani, A.; Pavan, G. M. *Nano Letters* **2011,** 11, (2), 723-728.
27. Santambrogio, P.; Cozzi, A.; Levi, S.; Rovida, E.; Magni, F.; Albertini, A.; Arosio, P. *Protein Expr. Purif.* **2000,** 19, 212-218.
28. Treffry, A.; Harrison, P. M. *Biochem. J.* **1978,** 171, 313-320.
29. Hennessy, D. J.; Reid, G. R.; Smith, F. E.; Thompson, S. L. *Canadian Journal of Chemistry* **1984,** 62, (4), 721-724.
30. Martyna, G. J.; Tobias, D. J.; Klein, M. L. *J. Chem. Phys.* **1994,** 101, 4177–4189.
31. Phillips, J. C.; Braun, R.; Wang, W.; Gumbart, J.; Tajkhorshid, E.; Villa, E.; Chipot, C.; Skeel, R. D.; Kalé, L.; Schulten, K. *Journal of Computational Chemistry* **2005,** 26, (16), 1781-1802.
32. Li, C.; Ellenburg, M.; Soistman, E.; Ruble, J.; Wright, B.; Ho, J.; Carter, D. *Acta Crystallographica Section D* **2006,** 62, 800-806.
33. Miyamoto, S.; Kollman, P. A. *J. Comput. Chem.* **1992,** 13, 952–962.
34. Andersen, H. J. *Comp. Phys.* **1983,** 52, 24–34.
35. Darden, T.; York, D.; Pedersen, L. J. *Chem. Phys. Lett.* **1993,** 98, 10089–10092.
36. Jorgensen, W. L.; Chandrasekhar, J.; Madura, J. D.; Impey, R. W.; Klein, M. L. *The Journal of Chemical Physics* **1983,** 79, (2), 926-935.
37. MacKerell, J., A. D. ; Bashford, D.; Bellott, M.; Dunbrack Jr., R. L.; Evanseck, J. D.; Field, M. J.; Fischer, S.; Gao, J.; Guo, H.; Ha, S.; Joseph-McCarthy, D.; Kuchnir, L.; Kuczera, K.; Lau, F.

T. K.; Mattos, C.; Michnick, S.; Ngo, T.; Nguyen, D. T.; Prodhom, B.; Reiher, I., W.E.; Roux, B.; Schlenkrich, M.; Smith, J. C.; Stote, R.; Straub, J.; Watanabe, M.; Wiorkiewicz-Kuczera, J.; Yin, D.; Karplus, M. *Journal of Physical Chemistry B* **1998,** 102, 3586-3616.
38. Beglov, D.; Roux, B. *Journal of Chemical Physics* **1994,** 100, 9050-9063.
39. Frisch, M. J.; Trucks, G. W.; Schlegel, H. B.; Scuseria, G. E.; Robb, M. A.; Cheeseman, J. R.; Montgomery, J. A.; Vreven, T.; Kudin, K. N.; Burant, J. C.; Millam, J. M.; Iyengar, S. S.; Tomasi, J.; Barone, V.; Mennucci, B.; Cossi, M.; Scalmani, G.; Rega, N.; Petersson, G. A.; Nakatsuji, H.; Hada, M.; Ehara, M.; Toyota, K.; Fukuda, R.; Hasegawa, J.; Ishida, M.; Nakajima, T.; Honda, Y.; Kitao, O.; Nakai, H.; Klene, M.; Li, X.; Knox, J. E.; Hratchian, H. P.; Cross, J. B.; Bakken, V.; Adamo, C.; Jaramillo, J.; Gomperts, R.; Stratmann, R. E.; Yazyev, O.; Austin, A. J.; Cammi, R.; Pomelli, C.; Ochterski, J. W.; Ayala, P. Y.; Morokuma, K.; Voth, G. A.; Salvador, P.; Dannenberg, J. J.; Zakrzewski, V. G.; Dapprich, S.; Daniels, A. D.; Strain, M. C.; Farkas, O.; Malick, D. K.; Rabuck, A. D.; Raghavachari, K.; Foresman, J. B.; Ortiz, J. V.; Cui, Q.; Baboul, A. G.; Clifford, S.; Cioslowski, J.; Stefanov, B. B.; Liu, G.; Liashenko, A.; Piskorz, P.; Komaromi, I.; Martin, R. L.; Fox, D. J.; Keith, T.; Laham, A.; Peng, C. Y.; Nanayakkara, A.; Challacombe, M.; Gill, P. M. W.; Johnson, B.; Chen, W.; Wong, M. W.; Gonzalez, C.; Pople, J. A., Gaussian 03, Revision D.02. 2004.
40. Vanommeslaeghe, K.; Hatcher, E.; Acharya, C.; Kundu, S.; Zhong, S.; Shim, J.; Darian, E.; Guvench, O.; Lopes, P.; Vorobyov, I.; Mackerell, A. D. *Journal of Computational Chemistry* **2010,** 31, (4), 671-690.
41. Vanommeslaeghe, K.; MacKerell, A. D. *Journal of Chemical Information and Modeling* **2012,** 52, (12), 3144-3154.
42. Vanommeslaeghe, K.; Raman, E. P.; MacKerell, A. D. *Journal of Chemical Information and Modeling* **2012,** 52, (12), 3155-3168.
43. Cross, J. P.; Lauz, M.; Badger, P. D.; Petoud, S. p. *Journal of the American Chemical Society* **2004,** 126, (50), 16278-16279.
44. Kaczorowska, M.; Cooper, H. *J Am Soc Mass Spectrom* **2009,** 20, (4), 674-681.
45. Mankbadi, M. R.; Barakat, M. A.; Ramadan, M. H.; Woodcock, H. L.; Kuhn, J. N. *The Journal of Physical Chemistry B* **2011,** 115, (46), 13534-13540.
46. Kleinman, M. H.; Flory, J. H.; Tomalia, D. A.; Turro, N. J. *The Journal of Physical Chemistry B* **2000,** 104, (48), 11472-11479.
47. Ottaviani, M. F.; Montalti, F.; Turro, N. J.; Tomalia, D. A. *The Journal of Physical Chemistry B* **1997,** 101, (2), 158-166.
48. Camarada, M. B.; Zúñiga, M.; Alzate-Morales, J.; Santos, L. S. *Chemical Physics Letters* **2014,** 616–617, (0), 171-177.
49. Chen, W. R.; Porcar, L.; Liu, Y.; Butler, P. D.; Magid, L. J. *Macromolecules* **2007,** 40, 5887–5898.
50. Liu, Y.; Bryantsev, V. S.; Diallo, M. S.; Goddard III, W. *J. Am. Chem. Soc.* **2009,** 131, 2798-2799.